

FULL PAPER

Structures, stabilities, and electronic properties of fullerene C₃₆ with endohedral atomic Sc, Y, and La: A dispersion-corrected DFT study

Alan Miralrio | Luis Enrique Sansores

Departamento de Materiales de Baja Dimensionalidad, Instituto de Investigaciones en Materiales, Universidad Nacional Autónoma de México, Apartado, Postal 70-360, México, DF 04510, Mexico

Correspondence

Luis Enrique Sansores, Departamento de Materiales de Baja Dimensionalidad, Instituto de Investigaciones en Materiales, Universidad Nacional Autónoma de México, Apartado, Postal 70-360, México, DF 04510, Mexico.

Email: sansores@unam.mx

Funding information

DGAPA for funding this research under project IN102616 and CONACYT for financial support (A. Miralrio scholarship).

Abstract

The M@C₃₆ compounds form a family of small endohedral metallofullerenes. Recently, these have been detected as the smallest endohedral compounds formed with Sc, Y, and La. For the first time, these compounds are studied theoretically. Calculations obtained at the dispersion-corrected DFT level PBE-D3(BJ)/def2-TZVP agree admirably with experimental results. The zero-point energy corrected binding energies can explain the lower abundance of La@C₃₆ in comparison with Sc@C₃₆ and Y@C₃₆. Their small HOMO-LUMO gaps denote high reactivity. The bond between Y and Sc with the cage is mostly covalent. In contrast, La is located at the fullerene's center with an ionic interaction; all metals transferred charge to the cage. Furthermore, La@C₃₆ was found in doublet state and the others preferred the quartet state. To conclude, according to the analysis of aromaticity performed by the NICS(0)_{iso} index, the insertion of none of these metals increase the aromaticity.

KEYWORDS

C₃₆ fullerene, density functional theory calculation, dispersion-corrected, electronic structure, endohedral fullerenes

1 | INTRODUCTION

Since the same year of their discovery,^[1] fullerenes have stood out for their capacity^[2] of trapping other species (atoms,^[3-5] molecules,^[3-5] or clusters^[6]) inside of them; hence, a large number of studies have been done.^[3-5] The internally doped fullerenes are known as endohedral fullerenes (EFs); being the endohedral metallofullerenes (EMFs) the most studied EFs, formed by C₆₀ or bigger cages, which contain lanthanide atoms as their endohedral species.^[3-6]

The most notable difference between hollow fullerenes and EFs is that the latter can violate the isolated pentagon rule (IPR).^[3-6] IPR establishes that a cage without adjacent pentagonal rings will form the most energetically favorable isomer of a hollow fullerene, however, EFs can violate this rule^[7] and several non-IPR endohedral fullerenes have been synthesized.^[3-6]

Despite the fact that, theoretically, C₂₀ is the smallest possible fullerene,^[8] its strained structure is not energetically favorable and the ring geometry is preferred^[9]; as a result, C₂₈ is the smallest fullerene detected in mass spectra.^[10] Moreover, other small fullerenes (smaller

than C₆₀) have been experimentally obtained^[11,12] and some have been predicted to be stable.^[13] Particularly, numerous experiments have been done on C₃₆ in gas phase.^[11,12,14-17] The HOMO-LUMO gap of several small fullerenes were measured by anion photoelectron spectroscopy.^[15] The gap of 0.8 eV, measured for C₃₆, agrees with that calculated (below than 0.5 eV) by a density-functional-based tight-binding method,^[15] due to the large error bar obtained in the experimental value.^[15] Similarly, C₃₂, C₄₄, and C₅₀ show large gaps and high stabilities.^[15] The D_{6h} and D_{2d} isomers (non-IPR) of C₃₆ have the minimal number of adjacent pentagonal rings among the 15 possible isomers.^[18] Both using density functional theory (DFT) studies were predicted to be quasi-isoenergetic in their singlet (D_{6h} and D_{2d}) and triplet (D_{6h}) states; nevertheless, the lowest energy isomer depends on the used methodology.^[19-27] Further calculations using CASSCF with single and multireference MP2 showed that the lowest isomer is the D_{6h} in singlet state.^[28] In addition, this study has proven that the lowest energy state has an important diradical character.^[28] Furthermore, it was demonstrated that both isomers can be transformed into each other by the Stone-Wales transformation.^[29]

C_{36} and other few solids have been observed in gas-phase, obtained by the arc-discharge method.^[30] Solid-state nuclear magnetic resonance (NMR) measurements suggest that the C_{36} has D_{6h} symmetry.^[30] In addition, its physical and chemical properties are consistent with covalent bonding between C_{36} molecules; in contrast, C_{60} forms a van der Waals solid. The formation of a partially hydrogenated molecule was reported as well, the $C_{36}H_6$.^[30] Scanning tunneling spectroscopy has been used to measure the band gap in C_{36} thin films.^[31] According to DFT calculations,^[31] the 0.8 eV of the measured band gap^[31] is due to the formation of dimers and trimers of C_{36} covalently bonded. This explains the lack of long-range order found in the thin films.^[31] Additionally, C_{36} was found more reactive than larger size fullerenes.^[31] Other theoretical studies have proposed different dimers^[32] and bidimensional crystals.^[33–35] The aromatic properties of D_{6h} - C_{36} , neutral and charged, were studied^[19,24,36] with nucleus independent chemical shift (NICS) calculations, performed with the gauge-independent atomic orbital (GIAO) method. According to these studies, neutral singlet D_{6h} - C_{36} is more aromatic than the triplet, and the hexagonal rings are locally more aromatic than pentagons.^[19] Another study on the aromatic character of C_{36} isomers and ions has concluded that their aromaticity is not related to the $2(N + 1)^2$ rule of spherical aromaticity,^[37] which predicts the increase of aromaticity in certain neutral and charged fullerenes.^[36]

Although the most studied EMFs are those formed by large cages (C_{60} or bigger),^[3–6] a few small EFs were experimentally obtained^[14,38,39] and studied theoretically.^[3,40,41] Currently, the smallest family of EMFs is $M@C_{28}$ ($M = Ti, Zr, Hf, \text{ and } U$).^[14,42] The following group was discovered with the detection of $La@C_{36}^+$ in laser vaporization of composites containing lanthanum and graphite.^[38] In consequence, $La@C_{36}^+$ is the smallest stable $La@C_{2n}^+$ EMF.^[43] Similarly, other EMFs were found with atomic Y, Sc, Gd, and Ce, engaged inside C_{36} .^[44] In these experiments, the most abundant species were $M@C_{44}$ and $M@C_{50}$,^[44] and the smallest were $Sc@C_{30}$, $M@C_{36}$ ($M = Y, La, Ce, Gd$) and $Ca@C_{44}$. These observations agree with the model based in terms of electronegativities and atomic radii (oxidation states 3+) proposed by Guo et al.^[40]

Recently, Dunk et al.^[39,42] did an extensive search of small EMFs, in which they reported the formation of small, medium, and giant EMFs in the gas-phase. These EMFs were obtained by laser evaporation of metal-incorporated graphite^[39,42] and were analyzed with high-resolution Fourier transform ion cyclotron resonance (FT-ICR) to determine their relative abundances. Dunk et al. propose that the formation of big fullerenes is due to a bottom-up mechanism; therefore, the growing of fullerenes takes place by C_2 insertions following a bottom-up transformation^[39,45]: $M@C_{28} \rightarrow M@C_{36} \rightarrow M@C_{44} \rightarrow M@C_{50} \rightarrow M@C_{60}$. These insertions are possible with high-temperature synthesis. Additionally, they have demonstrated that atomic U plays a very important role in the formation of $U@C_{28}$,^[42] catalyzing or nucleating its formation. Similarly, Dunk et al. infer that larger $U@C_{2n}$ fullerenes are formed based on $U@C_{28}$ as their precursor.^[42] As can be seen, small EMFs as $M@C_{28}$ and $M@C_{36}$ play an important role in the formation of bigger metallofullerenes. Despite the fact that currently many

$M@C_{36}$ have been detected in gas-phase ($M = U$,^[42] Th ,^[39] Sc ,^[39] Y ,^[39,44] La ,^[38,39,44] Ce ,^[39,44] Pr ,^[39] Nd ,^[39] Gd ,^[39,44] Tb ,^[39] Dy ,^[39] Ho ,^[39] Er ,^[39] and Lu ^[39]), only a few theoretical studies were done on them ($U@C_{36}$ ^[46] and $Y@C_{36}$ ^[47]). However, other EFs with C_{36} cage have been studied theoretically $X@C_{36}$ ($X = He$,^[48] Li ,^[32] C ,^[32] Ti ,^[49] V ,^[49] Cr ,^[49] Mn ,^[49] Fe ,^[49] Co ,^[49] Ni ,^[49] Cu ,^[49] H_2 ^[50]). The lack of studies about small endohedral metallofullerenes obtained in synthesis creates the necessity of intensifying the theoretical research to understand and predict their properties to compare them with future experiments. For that reason, this work describes for the first time group-3 elements (Sc, Y, and La) as an atomic endohedral dopant of C_{36} . Geometric, electronic, aromatic, and other properties are discussed.

2 | METHODS

Lowest energy structures of endohedral metallofullerenes $M@C_{36}$ ($M = Sc, Y, \text{ and } La$) were studied within a dispersion-corrected DFT methodology, using the generalized gradient approximation (GGA) of Perdew–Burke–Ermerhof^[51] (PBE) functional. The correction to the energy, due to dispersion interactions, was taken into account with the Grimme's (D3) term with Becke–Johnson (BJ)^[52] damping. The basis set used for all atoms was the triple- ζ valence basis set with one set of polarization functions def2-TZVP,^[53] which uses an effective core potential (ECP) to replace 28 core electrons for Y and 46 for La. In addition, the relativistic effects in these elements were taken into account with the scalar relativistic ECP. The method PBE-D3(BJ)/def2-TZVP was used in the Turbomole 6.5 code^[54] to obtain the optimized structures and other calculations. The integration grid size used was the finest grid size available: m5. To compare it with other calculations, C_{36} isomers, D_{6h} and D_{2d} were optimized in singlet and triplet states. The optimization procedure of the EMFs started from several structures with the endohedral atom located at different positions inside the D_{6h} - C_{36} with doublet and quartet multiplicities. Only lowest energy structures with all their vibrational frequencies have been reported. Furthermore, their potential energy surfaces (PES) were scanned in doublet, quartet, and sextet states with single point energy calculations as a function of the position of the endohedral atom throughout a relevant direction (from the fullerene's center to the center of the farthest hexagonal ring). Charge distributions were obtained from the density-based Hirshfeld population analysis using the wavefunction analysis program Multiwfn^[55] 3.3.7, with the output of a single point calculation of the lowest energy structures of each compound carried out with Gaussian 09^[56] at the level PBE-D3(BJ)/def2-TZVP.

Lowest unoccupied molecular orbitals (LUMO), highest occupied molecular orbitals (HOMO), electrostatic potential maps (ESP), and others, were plotted using the Gaussview 5 program.^[57] ESP was mapped over isosurfaces of 4×10^{-4} a.u. electron density. To analyze aromatic properties, NICS(0)_{iso} values were calculated using the NMR shielding tensor with the GIAO method. These values were obtained taking the negative of their isotropic coefficient and calculated at the centroid of several pentagonal and hexagonal rings, calculations were

TABLE 1 Comparison between 12 experimental^[55] and theoretical vibrational frequencies of Ar@C₆₀ endohedral fullerene

Method	Error ^a (%)
PBE/def2-TZVP	1.52
PBE-D3/def2-TZVP	1.47
PBE-D3(BJ)/def2-TZVP	1.46

^aThe error refers to the mean absolute percentage error obtained.

carried out using the program^[56] Gaussian 09 with the method GIAO/PBE-D3(BJ)/def2-TZVP. In addition, NICS(1)_{iso} and NICS(1)_{zz} have been obtained. NICS(1)_{iso} were calculated 1 Å above ring centers, taking the negative of the isotropic coefficient. NICS(1)_{zz} values were obtained taking the negative of the component perpendicular to the ring of the shielding tensor calculated 1 Å above ring centers.

To determine the stability of the compounds studied, the binding energy (BE_{ZPE}) was calculated as: $BE_{ZPE} = E_{ZPE}(M@C_{36}) - E(M) - E_{ZPE}(C_{36})$, where $E_{ZPE}(M@C_{36})$ refers to the total electronic energy of the isolated C₃₆-D_{6h} in doublet state plus the zero-point energy (ZPE) correction; $E(M)$ is the energy of the endohedral atom M in its atomic ground state ²D_{3/2}, and $E_{ZPE}(C_{36})$ is the energy of the endohedral compound fully optimized at the state indicated plus the corresponding ZPE. Additionally, vertical ionization energies (VIE) and vertical electron affinities (VEA) have been calculated.

To test the methodology used, the neutral I_h-C₆₀ in singlet state was optimized at the PBE-D3(BJ)/def2-TZVP level. Similarly to previous works,^[41,58] the method proposed was compared to the radius, single, and double bond lengths measured in I_h-C₆₀ by electron diffraction.^[59] PBE-D3(BJ)/def2-TZVP obtained an error (mean absolute percentage error) of 0.28%, improving slightly the uncorrected and previously used method PBE/def2-TZVP,^[41] with an error of 0.30%. In comparison with 14 experimental vibrational frequencies of C₆₀, measured by Fourier transform infrared spectroscopy (FT-IR),^[58] the proposed method obtained an error of 1.39%, quite better than the uncorrected result with an error of 1.48%.^[41] Likewise, the energetic properties predicted with the corrected method were tested with the fullerene I_h-C₆₀. The ionization energy obtained as 7.4 eV underestimated by 2.63% the 7.6 eV measured by electron impact techniques,^[60] which is equal to the uncorrected result without ZPE and dispersion correction. Similarly, the electron affinity, calculated as 2.6691 eV, underestimated by 0.54% the 2.6835 eV which was measured by laser photoelectron spectroscopy.^[61] A further comparison was made between PBE/def2-TZVP, the dispersion corrected PBE-D3/def2-TZVP without the damping term and the method used in this work. Table 1 shows the errors obtained from the three methods in comparison with 12 experimental vibrational frequencies obtained with FT-IR in the endohedral compound Ar@C₆₀. As can be seen, the error is reduced from 1.52% (obtained with the uncorrected method) to 1.46% (obtained with the proposed method). The inclusion of the term BJ-damping produces practically the same error than the method without damping (1.47%). According to Grimme et al., both variants are recommended in general, but the BJ-damping gives energies slightly

better to noncovalent interactions.^[52] In conclusion, the method PBE-D3(BJ)/def2-TZVP was used in this work because it gave more accurate results in the comparisons discussed above with regard to several tests previously reported.^[41]

3 | RESULTS AND DISCUSSION

3.1 | Isolated C₃₆-D_{6h}

To understand the formation of the endohedral fullerenes M@C₃₆ (M = Sc, Y, and La), we started this study with an analysis of the lowest energy structure of the neutral hollow fullerene C₃₆. As discussed in the introduction, the fullerene C₃₆ has 15 possible isomers^[18] and the most energetically favorable are D_{6h} and D_{2d} (Table 2). Both neutral isomers were optimized with the dispersion-corrected DFT methodology PBE-D3(BJ)/def2-TZVP, in singlet and triplet states. According to these calculations^[19-27] (Table 2), the lowest energy isomer is D_{6h} in singlet state, followed by D_{2d} singlet with an energy difference (taking into account the ZPE correction) $\Delta E_{rel} = 0.039$ eV. D_{2d} and D_{6h} isomers in triplet states have energy differences of 0.135 eV and 0.154 eV, respectively. In addition, the relative energies were calculated in the same way with the meta-GGA functional TPSS and the basis def2-TZVP, to ensure that these small energy differences can be calculated within the computational accuracy of the method proposed (Table 2). As in the previous calculations, D_{6h} in singlet state is the lowest energy isomer, followed by the D_{2d} in singlet state, with energy difference $\Delta E_{rel}^* = 0.015$ eV. With this method, the isomer D_{6h} in triplet state is lower in energy in comparison with the D_{2d} in triplet state, with relative energies of 0.090 eV and 0.193 eV, respectively (Table 2). So, according with both calculations, the D_{6h} in singlet state is the lowest energy isomer.

The small energy difference the isomers is consistent with previous DFT studies that have already predicted that both isomers are almost isoenergetic^[19-27]; the lowest energy isomer depends on the used methodology. The comparison made by Yuan et al.^[27] shows that the level used in the calculations is important to perform a realistic study. The Hartree-Fock (HF) method predicts the triplet D_{6h} isomer as the lowest energy state, similarly with the functionals B3LYP and B3PW91.^[27] Conversely, local-density approximation (LDA) and generalized gradient approximation (GGA) methods give as a result that the singlet D_{6h} is the lowest energy state.^[27] Our result is consistent with a complete active space self-consistent field (CASSCF) study with the single and multireference second-order Møller-Plesset perturbation theory (MP2), which obtained the D_{6h} isomer in singlet state as the lowest energy structure.^[28] According to this study, the wavefunction of the lowest energy state has an important diradical character; moreover, the electron correlation plays an important role to predict the D_{6h} singlet as ground state.^[28] Furthermore, as a consequence of an oversimplified form of the wavefunction,^[28] some methods can predict a C₃₆-D_{2d} isomer (denominated second-order Jahn-Teller distorted structure) as the lowest energy structure. Our open shell calculations do not show spin contamination according to the $\langle S^2 \rangle$ values obtained (Table 2); thus, the level of theory used is enough to describe

TABLE 2 Properties of D_{6h} and D_{2d} isomers of C₃₆ fullerene

Symmetry	M	ΔE_{rel} (eV)	ΔE_{rel}^* (eV)	HOMO-LUMO gap (eV)	$\langle S^2 \rangle$	VIE (eV)	VEA (eV)
D _{6h}	1	0.000	0.000	0.484	0.000	7.100	2.973
D _{2d}	1	0.039	0.015	0.412	0.000	6.757	2.708
D _{2d}	3	0.135	0.193	0.189	2.008	-	-
D _{6h}	3	0.154	0.090	0.092	2.023	-	-

Symmetry, multiplicity M, energy difference ΔE_{rel} (including ZPE) relative to the lowest energy system, ΔE_{rel}^* calculated at the level TPSS/def2-TZVP, HOMO-LUMO gap, $\langle S^2 \rangle$ value, VIE and VEA.

correctly the lowest energy state of the hollow C₃₆ without taking into account a multireferential method. Furthermore, NMR experiments describe the solid C₃₆ as covalently bonded D_{6h}-C₃₆ molecules.^[30] Similarly, infrared transmission spectrum^[30] of C₃₆ powder in KBr can be directly compared with the calculated infrared emission spectra of C₃₆-D_{6h} by LDA.^[27] In the following analysis, only the neutral singlet D_{6h} isomer is discussed.

Theoretical evidence suggests that the inclusion of the endohedral atom can change the cage geometry; Ti@C₃₆ has been obtained with the isomer D_{2d} as cage, with energy difference of 0.045 eV respect to the D_{6h} cage calculated with the BP86 functional and triple- ζ + polarization Slater-type basis functions. As well, both cages charged with 4 electrons were found isoenergetic.^[45] In addition, both isomers of Ti@C₃₆ can be related by Stone-Wales transformations,^[45] similarly to the C₃₆.^[29] For these reasons, both isomers have been taken into consideration as cages.

Due to symmetry considerations, the neutral C₃₆-D_{6h} isomer has only four different C—C bond lengths (Figure 1). The (5:5)_A bonds, which connect two pentagonal rings, have the shortest bond length 1.415 Å. These bonds form two hexagonal rings (named h_A in subsequent references) perpendicular to the C₆ axis of symmetry. The longest bond length corresponds to the (6:6) bonds, which connect two hexagonal rings, with length 1.493 Å. Intermediate bond lengths were obtained from (5:6) and (5:5)_B bonds: 1.434 Å and 1.440 Å, which connect a pentagonal ring with a hexagonal ring and two pentagonal rings. These form the remaining six hexagonal rings (h_B) around the C₆ axis of symmetry. As can be seen in Figure 1, h_A rings have the shortest bond lengths of all, comparable to the C—C bond lengths in benzene 1.40 Å.

The molecular orbitals (Figure 2) that belong to C₃₆ show π bonding orbitals on its HOMO and antibonding π orbitals with a nodal plane perpendicular to the C₆ axis of symmetry. HOMO and LUMO correspond to single degenerate states: 5b_{1u} and 5b_{2g}. Interestingly, both HOMO and LUMO around the h_A rings are very similar to the antibonding benzene orbital B_{1g}. Moreover, HOMO-1 is a doubly degenerate orbital e_{1g}, very similar to the bonding orbital e_{1g} in benzene. Likewise, LUMO + 1 orbital E_{2g} resembles the benzene antibonding orbital e_{2u}. The local similarity will be used to compare it with the benzene and its complexes with metals. The HOMO-LUMO gap was calculated as 0.484 eV within the experimental error of 0.8 eV, measured in molecular C₃₆ by anion photoelectron spectroscopy.^[15] Yuan et al. obtained that the calculated HOMO-LUMO gaps depend strongly on

the methodology used,^[15] obtaining gaps above 1.4 eV with HF, B3LYP, and B3PW91.^[27] In contrast, LDA and GGA approaches^[27] obtained values around 0.5 eV, which can be compared with the experimental measure.^[15] According to scanning tunneling spectroscopy experiments,^[31] the band gap in solid C₃₆ is 0.8 eV. DFT calculations have proved that this band gap is the result of the formation of dimers and trimers of C₃₆ molecules covalently bonded. In addition, the relationship between a small gap and high reactivity^[62] can explain the high reactivity experimentally observed^[31] in molecular C₃₆. Other possible structures have smaller gaps (Table 2); this statement agrees with the correlation between HOMO-LUMO gap, stability and chemical reactivity^[62,63] so that the most stable fullerene isomer tends to have the largest HOMO-LUMO gap.^[63] From photoelectron spectroscopy,^[15] the VEA was estimated to be 2.8 eV,^[27] which agrees with the 2.973 eV reported in Table 2. The lowest energy structure has the biggest VIE and VEA, 7.100 eV and 2.973 eV, in comparison with the D_{2d} structure with values 6.757 eV and 2.708 eV, respectively.

According to the Hirshfeld charge distribution (Figure 3), the hexagonal rings, perpendicular to the C₆ axis, have more negative charge with values -0.010. Equivalently, the ESP map shows its most negative region around these rings (Figure 3). The most positive Hirshfeld charges (0.008) are located in the atoms nearest to the hexagonal rings mentioned above; this fact results in an ESP almost neutral around these regions. It is interesting that this accumulation of charge could produce an electrostatic potential suitable to produce a cation- π interaction^[64] with certain atoms as: Li⁺, Na⁺, K⁺, or Al⁺. These kind of compounds have been previously theoretically studied.^[32] Furthermore, it is expected an interaction between these h_A hexagonal rings and the metals proposed by their benzene-like properties (Sc, Y, and La).

The magnetic indices of aromaticity NICS(0)_{iso}, NICS(1)_{iso} and NICS(1)_{zz} were used in this work to study the aromatic properties of the proposed systems. Table 4 lists the values calculated for the hollow fullerene C₃₆-D_{6h}. According to their negative NICS(0)_{iso} (Table 4), all the rings in C₃₆ have aromatic character. The most negative value (-20.41 ppm) obtained for the hexagonal rings h_A, perpendicular to the C₆ axis, denotes a more aromatic character in comparison with h_B rings, with values -7.16 ppm. NICS(1)_{iso} and NICS(1)_{zz} show similar results, with the most negative indices for the h_A, with values -6.96 ppm and -21.47 ppm, respectively. According with these indices, h_B and pentagonal rings are nonaromatic or slightly antiaromatic (Table 4). Calculations made at GIAO-HF/6-311(d)^[24] and GIAO-B3LYP/6-31G

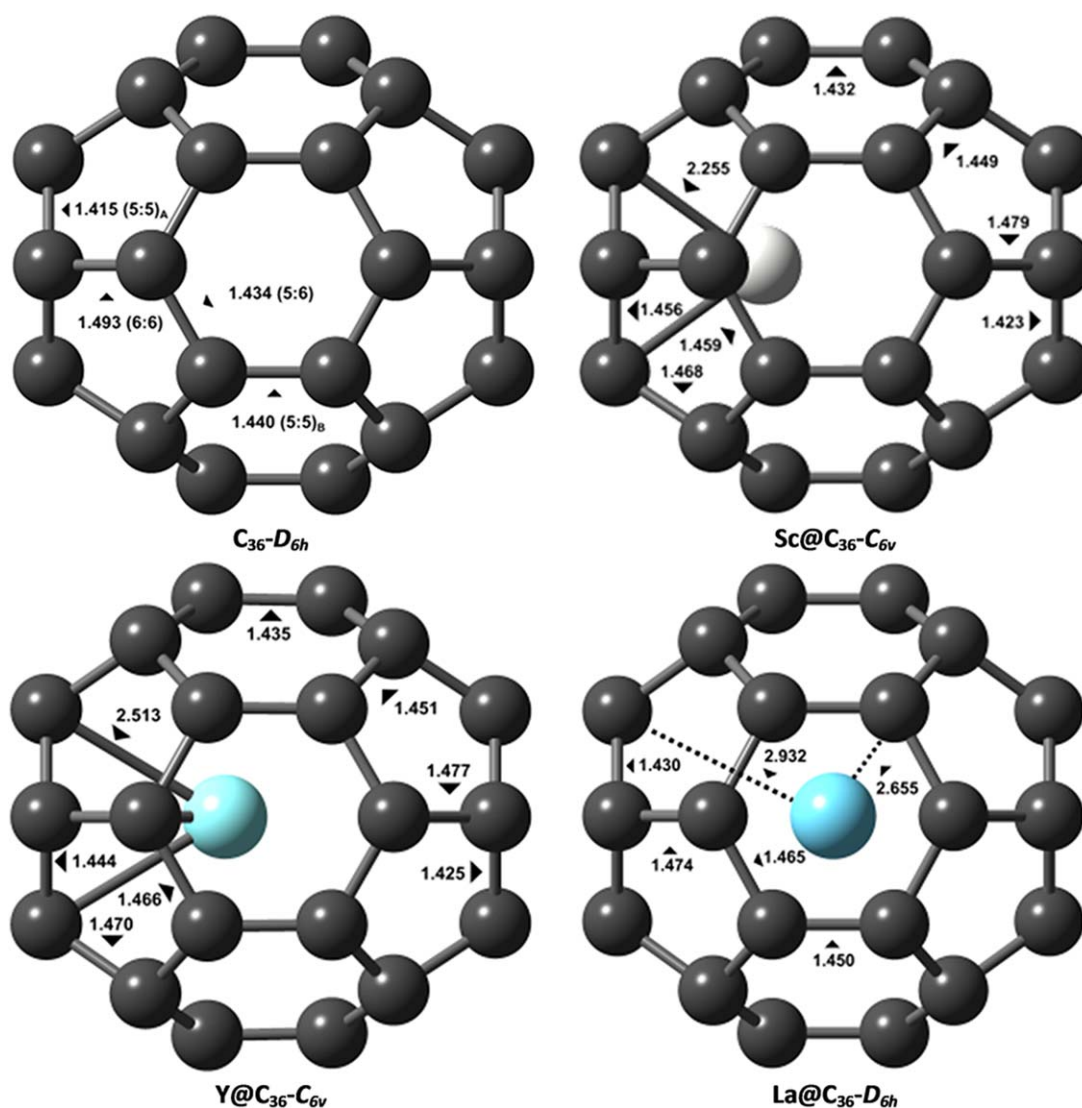


FIGURE 1 Optimized geometries obtained at the level PBE-D3(BJ)/def2-TZVP for: singlet $C_{36}-D_{6h}$, quartet $Sc@C_{36}-C_{6v}$, quartet $Y@C_{36}-C_{6v}$, and $La@C_{36}-D_{6h}$ doublet. Bond lengths in Angstroms (\AA)

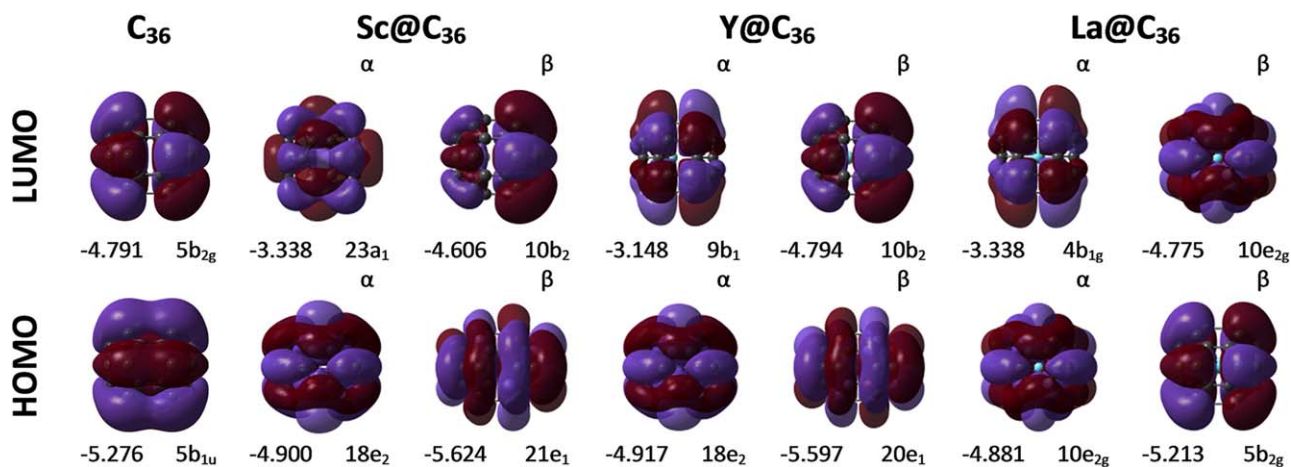


FIGURE 2 HOMOs and LUMOs of $C_{36}-D_{6h}$ fullerene and $M@C_{36}$ ($M = Sc, Y, \text{ and } La$) in their lowest energy state. Degenerated states are shown as the superposition of orbitals. Orbital label and related energies in eV annotated below. Isovalues: 5×10^{-3} a.u

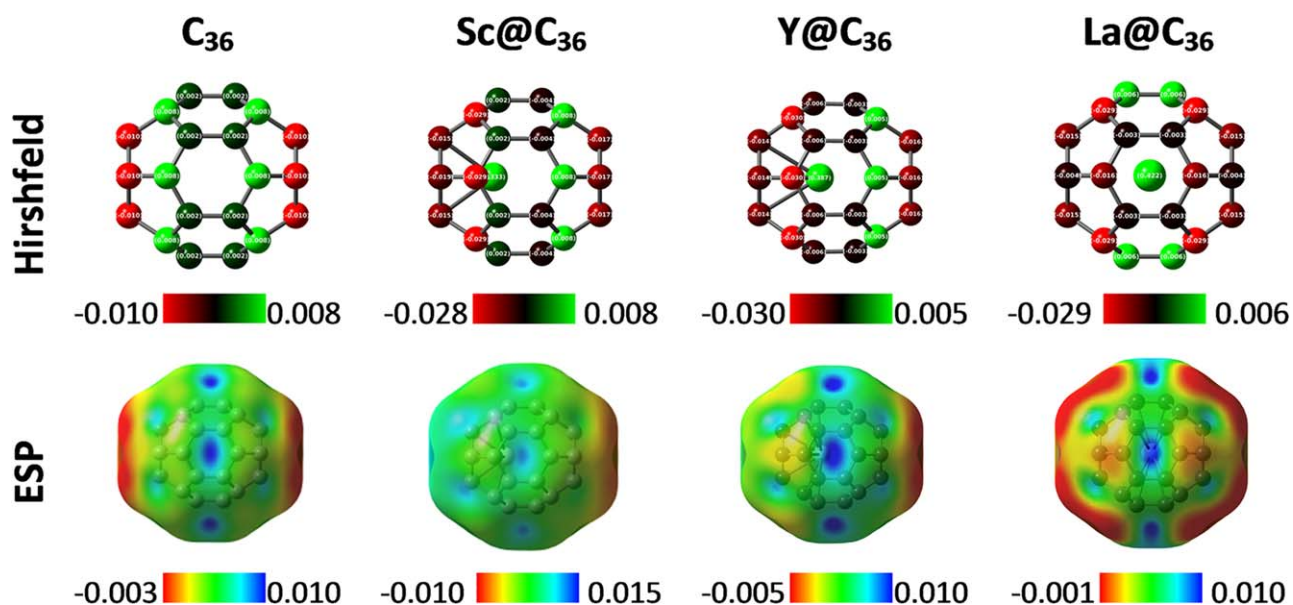


FIGURE 3 Hirshfeld charge distributions and ESPs of neutral singlet $C_{36}\text{-D}_{6h}$ and $M@C_{36}$ ($M = \text{Sc}, \text{Y},$ and La). ESP mapped over the isosurface with an electron density of 4×10^{-4} a.u.

(d)^[65] levels of theory obtained very similar results, including the strongest aromatic character in the h_A rings. Pentagonal rings obtained values -3.54 ppm. These values are completely consistent with previous calculations.^[19,24,36] According to Kerim et al., a correlation does not exist between the NICS calculated at the center of C_{36} isomers and the most stable structure.^[37] Additionally, the $2(N + 1)^2$ rule is not associated with aromaticity in these isomers; therefore, the $\text{NICS}(0)_{\text{iso}}$ can be related only to local aromaticity. Moreover, aromatic stabilization could not play an important role in these systems as in other fullerenes and EMFs.

3.2 | Lowest energy structures and geometries of $M@C_{36}$

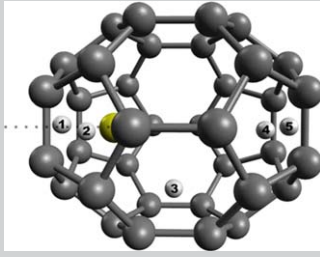
We have studied $M@C_{36}$ EMFs with the group-3 elements Sc, Y, and La. The search for their lowest energy structures started with the

optimization of several geometries with the endohedral atom located at different positions inside the fullerene $C_{36}\text{-D}_{6h}$. In addition, optimizations with the $C_{36}\text{-D}_{2d}$ isomer as cage were carried out. The structures were optimized with doublet and quartet multiplicity. In addition, their PESs were scanned in both states and in sextet as a function of the distance from the endohedral atom to the center of the h_A ring. We report only the lowest energy structure (taking into account the ZPE correction) with all vibrational frequencies obtained as real. Moreover, none show spin contamination according to the $\langle S^2 \rangle$ values obtained on each calculation (Table 3). Negative HOMO-LUMO gaps in Table 3 are due to the occupation used to obtain quartet and sextet multiplets. Higher energy alpha orbitals are occupied and Lower energy beta orbitals are unoccupied in these cases. Due to the lack of studies on these systems, we propose two complementary reference systems: metal-benzene complexes $M\text{-C}_6\text{H}_6$ ^[66–69] and EMF derivatives of $M@C_{82}$

TABLE 3 Properties of $M@C_{36}$ ($M = \text{Sc}, \text{Y},$ and La)

$M@C_{36}$	Symmetry	M	ΔE_{rel} (eV)	ΔE_{rel}^+ (eV)	Δr (Å)	$\langle S^2 \rangle$	BE_{ZPE} (eV)	HOMO-LUMO Gap (eV)	VIE (eV)	VEA (eV)	Hirshfeld charge
Sc@ C_{36}	C_{6v}	4	0.000	0.000	0.794	3.772	-5.726	0.294	6.866	2.774	0.333
Sc@ C_{36}	C_{6v}	2	0.156	0.207	0.766	0.752	-5.570	0.133	6.611	2.973	0.348
Sc@ C_{36}	C_{6v}	6	2.232	1.718	0.878	8.781	-3.494	-2.02	-	-	-
Y@ C_{36}	C_{6v}	4	0.000	0.000	0.505	3.764	-5.549	0.123	6.745	2.970	0.387
Y@ C_{36}	C_{6v}	2	0.024	0.062	0.418	0.751	-5.524	0.112	6.622	2.989	0.425
Y@ C_{36}	C_{6v}	6	2.040	1.980	0.343	8.763	-3.508	-2.05	-	-	-
La@ C_{36}	D_{6h}	2	0.000	0.000	0.000	0.750	-4.946	0.105	6.702	3.077	0.422
La@ C_{36}	D_{6h}	4	0.054	0.012	0.000	3.758	-4.891	-0.018	6.586	3.242	0.421
La@ C_{36}	D_2	6	1.988	1.774	0.000	8.762	-2.958	-1.915	-	-	-

Symmetry, multiplicity M, energy difference ΔE_{rel} (including ZPE) relative to the lowest energy system, ΔE_{rel}^+ calculated at the level TPSS/def2-TZVP off center displacement Δr of M, $\langle S^2 \rangle$ value, binding energy BE_{ZPE} , HOMO-LUMO gap, VIE, VEA, and Hirshfeld charge.

TABLE 4 NICS(0)_{iso}, NICS(1)_{iso}, and NICS(1)_{zz} values^a of neutral singlet C₃₆ and M@C₃₆ (M = Sc, Y, and La) calculated at each ring center


	Ring 1	Ring 2	Ring 3	Ring 4	Ring 5
C ₃₆	-20.41 (-6.96) -21.47	-3.54 (0.26) 4.70	-7.16 (0.15) 2.98		
Sc@C ₃₆	-16.98 (-2.41) -3.59	-4.69 (-0.17) -1.32	1.78 (3.47) 10.90	1.42 (3.47) 2.11	-11.29 (-1.94) -4.98
Y@C ₃₆	6.04 (0.28) 1.96	-9.96 (1.99) 1.46	30.73 (2.62) 7.72	-20.62 (1.37) 0.97	-47.67 (-0.71) -2.98
La@C ₃₆	3.88 (4.21) 1.44	-5.83 (-1.42) 0.51	-16.00 (-1.98) -6.04		

^aNICS(0)_{iso} values on the left, NICS(1)_{iso} values between parentheses and NICS(1)_{zz} on the right, values in ppm.

C_{2v}(82) with adamantylidene (Ad)^[70-72], both interacting with the studied metals (Sc, Y, and La). It is a known fact that benzene can bond with d-block metals creating compounds similar to Cr(C₆H₆)₂.^[73] Complexes M= (Sc, Y, and La)-C₆H₆ have been previously, experimentally and theoretically studied^[66-69]; hence, these compounds will be used as a frame of reference in this study. Cr(C₆H₆)₂ was chosen because its properties have been measured more precisely than the isolated EMFs.^[74-77] The shortest distance M-C is discussed in detail for each case.

Sc@C₃₆ was obtained in quartet state with C_{6v} symmetry (Table 3). The Sc atom was displaced 0.794 Å from the fullerene's center in direction of a h_A ring, which bond lengths increased to 1.456 Å (Figure 1); the Sc-C distances were 2.255 Å (Figure 1). In comparison, Sc-benzene was found experimentally in quartet state^[66] and Sc-C distance from Sc-benzene was calculated^[66] as 2.44 Å at the level B3LYP/6-311 + G(d). Additionally, Sc-C bond length in Sc@C₈₂-C_{2v}(9) (Ad) was experimentally determined as 2.323 Å by single crystal X-ray diffraction.^[72] Similarly to Sc@C₃₆, the Sc in Sc@C₈₂-C_{2v}(9)(Ad) is located over a hexagonal ring^[72] which is on the tip of the fullerene cage. Moreover, the quartet state in Sc@C₃₆ is followed by doublet and sextet with relative energies 0.156 eV and 2.232 eV, both with C_{6v} symmetries (Table 3). The relative energies calculated with the TPSS/def2-TVZP method follow the same order, with the quartet state followed by doublet and sextet, with relative energies of 0.207 eV and 1.718 eV, respectively. A C_s symmetry structure in doublet state was obtained from the D_{2d} cage, 0.067 eV above the lowest energy minimum (Supporting Information Table S1).

Similar to the previous compound, Y@C₃₆ has quartet state and symmetry C_{6v}. Y is displaced from the center by 0.505 Å in direction of a h_A ring (Figure 1). The Y-C distance is longer than the previous compound and was calculated as 2.513 Å (Figure 1). This distance is entirely comparable with the one obtained for Y-benzene (distance Y-C = 2.524 Å) in quartet state and symmetry C_{6v} from MP2 calculations.^[68] In addition, the Y-C distance 2.475 Å measured by single

crystal X-ray diffraction in Y@C₈₂-C_{2v}(9)(Ad) is quite similar.^[71] As in the previous EMF, the Y atom is located over a hexagonal ring along the C₂ axis of symmetry. Moreover, according to experimental and theoretical studies, the lowest energy structure for Y-Benzene has doublet state and C_{2v} symmetry due to a pseudo Jahn-Teller distortion.^[68] This structure is followed by the quartet with energy difference 0.497 eV,^[68] calculated at the CCSD(T)//MP2 level. The C_{6v} in doublet state has all its vibrational frequencies real and is 0.024 eV higher in energy, followed by the sextet with 2.040 eV above the ground state (Table 3). In addition, the TPSS/def2-TZVP calculation obtained the same order, with the quartet followed by doublet and sextet, with energy differences of 0.062 eV and 1.980 eV (Table 3). Both quartet and doublet states could appear in experiments due to the small energy difference; however, according to our results, the C_{6v} quartet structure is preferred. Taking the D_{2d} isomer as cage, a C_s symmetry structure in doublet was obtained with an energy difference of 0.040 eV relative to the lowest energy minimum (Supporting Information Table S1).

Contrastingly, La@C₃₆ has been found in doublet state and with symmetry D_{6h} (Table 3). Quartet C_{6v} and sextet D₂ have energy differences of 0.054 eV and 1.988 eV, respectively. Similarly, the TPSS/def2-TZVP calculation found the doublet state followed by quartet and sextet states, with relative energies calculated as 0.012 eV and 1.774 eV, respectively (Table 3). In this case, the inclusion of La in the D_{2d} cage resulted in a C_{2v} structure in doublet state, 0.023 eV above the D_{6h} doublet (Supporting Information Table S1). As can be seen, the inclusion of La reduces the energy difference between the isomers, in similar way to Ti@C₃₆ and the tetraanion C₃₆⁴⁻. So, the donation of charge from the metal to the cage could result in a cage more energetically favorable to host the atom, different from the lowest energy isomer.

As in the previous benzene compound, the La-benzene has a pseudo Jahn-Teller distortion, symmetry C_{2v} and doublet state.^[68] According to CCSD(T)//MP2 calculations, the quartet state is closer to a doublet state, with relative energy 0.324 eV above the ground state.^[68] The La atom is located at the fullerene's center and the La-C

distance is 2.655 Å (Figure 1); moreover, both are related to the h_B rings, the La atom is closer to the h_B rings than to the h_A (Figure 1). In La-Benzene, the distance La-C is 2.659 Å for the C_{6v} in quartet state^[68]; no doublet state was reported. Finally, the La-C distance was measured^[70] as 2.658 Å in La@C₈₂-C_{2v}(9)(Ad). As can be seen, these distances La-C are almost equivalent.

Similarly to the endohedral compounds formed by C₈₂-C_{2v}(9)(Ad),^[70-72] the increase in M-C distance can be understood in terms of the ionic radii of M³⁺. Sc has ionic radii of 0.81 Å, it is followed by Y with radius 0.91 Å and finally La with 1.15 Å. The on center position of La is a consequence of its largest size. This agrees with the model-based electronegativities and atomic radii (oxidation states 3+) proposed by Guo et al.^[40]

Both Sc@C₃₆ and Y@C₃₆ increased the C-C distances in h_A rings, whereas there is a reduction in the case of h_B rings. In contrast, the h_B rings in La@C₃₆ increase more their C-C distances than h_A rings. This elongation in C-C distances was found as well in metal-benzene complexes.^[66-69]

3.3 | Energetic properties and molecular orbitals

Recently, Dunk et al. reported the formation of small, medium and giant EMFs of many elements,^[39] presenting the FT-ICR mass spectrum as a function of the number of carbon atoms for all EMFs.^[39] In the case of the EMFs formed with M = Sc, Y, and La, they obtained the compounds M@C₃₆ as the smallest possible EMFs. Their relative abundances show that the smallest compounds M@C₃₆ are not as abundant as the bigger ones: M@C₄₄ and M@C₅₀.^[39] What is interesting is the fact that La@C₃₆ showed a lower abundance in comparison with Sc@C₃₆ and Y@C₃₆.^[39] In contrast, both Sc@C_{2n} and Y@C_{2n} have very similar abundances, particularly in Sc@C₃₆ and Y@C₃₆. As in other studies, we calculated the binding energy BE_{ZPE} to analyze stability^[41]: Sc@C₃₆ has the highest BE_{ZPE}, calculated as -5.726 eV (Table 3), followed closely by Y@C₃₆ with BE_{ZPE}(Y@C₃₆) = -5.549 eV (Table 3). Finally, La@C₃₆ has the lowest BE_{ZPE} with value -4.946 eV (Table 3), considerably less than the other compounds. Hence, we have obtained binding energies that follow an order BE_{ZPE}(La@C₃₆) < BE_{ZPE}(Y@C₃₆) ~ BE_{ZPE}(Sc@C₃₆), which are very similar to the experimental relative abundances found for M@C₃₆ (M = Sc, Y, and La).^[39] According to that, the relative abundance observed in experiments is the result of the energetically favorable inclusion of metallic atoms. This increases the stability of the whole compound, particularly with Sc and Y.

To study the reactivity of the compounds, we have calculated the HOMO-LUMO gap. This has proved to have a direct relationship with the chemical reactivity,^[62] particularly in fullerenes.^[63] As can be seen in Table 3, the lowest energy structures for each M@C₃₆ have the largest HOMO-LUMO gaps, however, all of them are smaller than gap 0.484 eV (Table 2), found in the isolated fullerene C₃₆-D_{6h} in singlet state. Moreover, the orbitals that belong to metal-benzene complexes are a simple and convenient approximation to the molecular orbitals in M@C₃₆. A metal atom M = Sc, Y, or La with ground state ²D_{3/2}, which interacts with a benzene molecule C₆H₆-D_{6h} in singlet state, can form an M-Benzene complex in quartet state with symmetry C_{6v}, in spite of

the pseudo Jahn-Teller distortion experimentally observed.^[68] The overlap between metal and benzene orbitals forms three kinds of bonds between them: the doubly degenerate benzene orbital e_{2u} interacts with the metal orbitals d_{xy} and d_{x²-y²}, the overlap between them forms a δ between the metal and the benzene and the resultant doubly degenerate antibonding orbital e₂ is occupied by two unpaired electrons; the remaining singly occupied bonding orbital a₁ is formed by the contributions of metal orbitals s, d_{z²} and the benzene orbital; finally, the doubly degenerate benzene orbital e_{1g} with the d_{yz} and d_{xz} metal orbitals create π bonds between benzene and the metal, obtaining the unoccupied bonding orbital e₁. The remaining benzene orbital b_{1g} is not bonding with the metal. Moreover, the other orbitals deeper in energy are doubly occupied bonding orbitals and form the bonds described above.

Sc@C₃₆ has the largest HOMO-LUMO gap with a value 0.294 eV that corresponds to HOMO α and LUMO β . Figure 2 shows that HOMO α is a doubly degenerate state 18e₂ which forms δ bonds between Sc and a h_A ring, such as the metal-benzene orbital e₂. Likewise, HOMO β is a doubly degenerate state 21e₁ (Figure 2), where Sc forms π bonds with the cage. LUMO α is the single degenerate 23a₁ and has contributions from the d_{z²} orbital of Sc, with π bonds over the whole cage (Figure 2). Similarly to other cases, orbital 23a₁ resembles locally the a₁ of a metal-benzene complex with the σ bond between the metal and the ring. LUMO β is the singly degenerate state 10b₂ and shows π bonds over the cage but with a nodal plane perpendicular to the C₆ axis of symmetry. In addition, this orbital resembles locally the benzene orbital b_{1g} around h_A rings (Figure 2).

In relation to Y@C₃₆, its HOMO α is the doubly degenerate state 18e₂, and, as in previous compounds, resembles locally the metal-benzene e₂ with the formation of a δ between Y and a h_A ring. Similarly, HOMO β is a doubly degenerate state 20e₁ (Figure 2), which locally resembles the metal-benzene orbital e₁ with π bonds between Y and a h_A ring. Both HOMO α and HOMO β show π bonds over the whole fullerene. Contrastingly, LUMO α and LUMO β do not show bonds between Y and the cage; additionally, these orbitals correspond to states 9b₁ and 10b₂ (Figure 2). As expected, both LUMO α and LUMO β orbitals locally resemble the benzene orbital b_{1g}. In this case, the HOMO-LUMO gap between HOMO α and LUMO β was calculated as 0.123 eV, being the largest in comparison to the other Y@C₃₆ structures (Table 3).

Finally, the HOMO α in La@C₃₆ is the doubly degenerate state 10e_{2g} (Figure 2). This orbital does not show contributions of the endohedral atom and locally resembles the benzene orbital e_{2u}. Similarly, HOMO β does not show contributions between La and the cage and is almost equal to the LUMO of the hollow C₃₆. In addition, LUMO α does not have a bond between La and the cage; instead, it has π bonds over the whole cage and a nodal plane perpendicular to the 6-fold axis. Equivalently, LUMO β has no bond between the endohedral atom and the cage; in fact, the contributions between La and the cage appear definitely deep in energy, up to HOMO α -6 and HOMO β -5 corresponding to states 9a_{2u} (Figure 2). The HOMO-LUMO gap between HOMO α and LUMO β is the smallest of the three analyzed compounds with value 0.105 eV.

The bond lengths and interactions showed by Sc@C₃₆ and Y@C₃₆ are consistent with the formation of covalent bonds between the metal atom and the cage; whereas the La atom in La@C₃₆ does not interact covalently and is consistent with an ionic interaction similar to other EMFs.^[41] This could be explained by the lower ionization energy of La (5.58 eV) in comparison with Sc and Y (6.56 eV and 6.21 eV, respectively) so that the valence electrons from La can be easily transferred to the cage, fully filling the benzene state 5b_{2g} (Figure 2) and leaving the state 10e_{2g} (Figure 2) with an unpaired electron.

The small HOMO-LUMO gap in the studied systems (Table 3) indicate a high reactivity in all of them^[63]; additionally, their gaps follow the same order of the binding energies. Together, these systems give some evidence of the possible formation of bigger EMFs by a bottom-up mechanism due to their high reactivity.^[39] As it is shown in Table 3, both the BE_{ZPE} and HOMO-LUMO gap follow the same order with the lowest values for La@C₃₆ and the highest for Sc@C₃₆. Similarly, the vertical ionization energy decreases from Sc@C₃₆ to La@C₃₆, with values 6.866 eV and 6.702 eV, respectively (Table 3). In the middle is Y@C₃₆ with VIE = 6.745 eV; thus, the most stable compounds tend to have higher VIEs. Conversely, the vertical electron affinity calculated for these compounds follow the inverse order: Sc@C₃₆ has the lowest VAE, with value 2.774 eV, followed by Y@C₃₆ with 2.970 eV and La@C₃₆ with 3.077 eV, the highest VAE.

3.4 | Charge distributions and ESP maps

The electrostatic potential and the charge distribution provide information about the transferred charge between an endohedral species and the cage. In comparison with the other compounds (Table 3), the Sc atom in Sc@C₃₆ transfers the smaller charge to the cage. Sc is positively charged with a Hirshfeld charge of 0.333, which was mainly transferred to the first neighbors of the h_A ring bonded to Sc (Figure 3). The transferred charge creates a region with ESP almost neutral around the h_B rings; whereas the h_A ring opposite to Sc shows an ESP negative, similar to the ESP around the h_B rings in the hollow fullerene C₃₆ (Figure 3).

Y@C₃₆ is similar to Sc@C₃₆ (Figure 3), which has an ESP almost neutral around the h_B rings with positive regions at their center. The Y atom has a positive charge of 0.387, which was mainly transferred to the first neighbors as in the previous case of Sc@C₃₆. The accumulation of charge made a slightly negative region around the atoms of h_B ring. Moreover, the region near the h_A ring opposite to the Y atom shows the most negative ESP.

The La atom inside La@C₃₆ (Figure 3), with charge 0.422 (Table 3), shows the greatest positive charge of all the studied compounds. As shown in the molecular orbital analysis, the interaction between La and the cage is omnidirectional and its valence electrons were completely transferred to fill the cage orbitals. This suggests a pure ionic interaction between La and the cage, similar to that observed in La³⁺@C₈₂³⁻-C_{2v}(9).^[76] As in previous cases, the charge was mainly accumulated in the first neighbors of the two h_A rings, remaining only four carbon atoms positively charged with charge 0.006. The ESP shows a neutral region around the h_B rings with positive potential energy at their cen-

ters. The most negative ESP (Figure 3) shows that the regions near the carbon atoms have the greatest negative charge. In conclusion, the interaction between the endohedral atom and the cage can be described as partially covalent and ionic for Sc@C₃₆ and Y@C₃₆. In contrast, the metal-cage interaction in La@C₃₆ agrees with a pure ionic type.

In addition, the charge transfer between the endohedral species and the cage has influence on the position of the metal atom. This has been reported previously in similar metal-gold cage compounds.^[78,79] In case of Sc@C₃₆ and Y@C₃₆, both metals donate less charge (0.333 and 0.387, respectively) to the cage and are more displaced off center (0.794 Å and 0.878 Å, respectively) in its lowest energy structure (quartet and symmetry C_{6v}) in comparison with their doublet states, with charges 0.348 and 0.425, respectively, and off center displacements of 0.766 Å and 0.418 Å, respectively (Table 3). Structures with Sc or Y located on-center have imaginary frequencies and cannot be taken into consideration. Thus, a lower donation of charge from the metal to the cage is energetically preferred in both cases and a higher donation of charge results in a less displaced metal into the cage. In case of La@C₃₆, doublet and quartet states have the La located on-center, with symmetries D_{6h}. In both cases, La donates almost the same charge (0.422 and 0.421, respectively). No structure with La located off-center was found. Overall, the donation of charge increases from Sc to La, as well as decreases the off-center displacement.

3.5 | Aromaticity

As previously discussed, the C₃₆ does not obey the rule 2(N + 1)² of spherical aromaticity^[37] and all its rings are locally aromatic according to all their negative NICS(0)_{iso} (Table 4). We have studied the aromatic properties of all M@C₃₆ compounds to establish whether the endohedral doping increases their aromaticity (as X@C₂₈) with per example endohedral group-4 atoms.^[41] This analysis was made considering the five different rings of compounds with C_{6v} symmetry and three different metals for the D_{6h} symmetry (Table 4).

In the case of Sc@C₃₆, the hexagonal ring h_A bonded to Sc (Ring 1) and the other h_A ring (Ring 5) decreases their aromatic character with NICS(0)_{iso} values of -16.98 ppm and -11.29 ppm (Table 4). In contrast, the pentagonal rings near to Sc (Ring 2) slightly increased their aromatic character with NICS(0)_{iso} -4.69 ppm. Interestingly, even though the hexagonal rings h_B (Ring 3) are aromatic in the hollow fullerene, they are nonaromatic or slightly antiaromatic in this endohedral compound with NICS(0)_{iso} 1.78 ppm. Similarly, the remaining pentagonal rings (Ring 4) far away from the Sc atom are nonaromatic or slightly antiaromatic with positive NICS(0)_{iso}, calculated as 1.42 ppm (Table 4). In addition, NICS(1)_{iso} and NICS(1)_{zz} indices agree with these behavior (Table 4).

Similar to the previous case, the h_A ring close to Y (Ring 1) in Y@C₃₆ decreased its aromatic character; moreover, according to their positive NICS(0)_{iso} value (6.04 ppm), these rings are antiaromatic. Equivalently, the h_B rings (Ring 3) have an antiaromatic character according to their positive NICS(0)_{iso} values (30.73 ppm). Contrastingly, the other rings increased considerably their aromatic character; for

instance, the h_A ring opposite to Y (Ring 5) has increased its aromatic character with a large negative NICS(0)_{iso} of -47.67 ppm (Table 4). Moreover, both pentagonal rings close to Y and the other rings increased their aromatic character with negative NICS(0)_{iso} values -9.96 ppm and -20.62 ppm, respectively (Table 4). In addition, NICS(1)_{iso} and NICS(1)_{zz} indices agree with these behavior (Table 4). Mainly NICS(1)_{iso} and NICS(1)_{zz} agree with the character detailed previously. According with both indices, the pentagonal rings (rings 2 and 4) are antiaromatic due to their positive values (Table 4).

In La@C₃₆, both rings h_A (Ring 1) are antiaromatic according to their positive NICS(0)_{iso}, calculated as 3.88 ppm (Table 4); whereas its pentagonal (Ring 2) and hexagonal rings h_B (Ring 3) have aromatic character with NICS(0)_{iso} values -5.83 ppm and -16.00 ppm. Similarly, NICS(1)_{iso} and NICS(1)_{zz} have values that are consistent with these character (Table 4). As an exception of the above, the NICS(1)_{zz} = 0.51 ppm calculated for pentagonal rings (Ring 2) denotes a slightly antiaromatic character or nonaromatic. Despite of that, NICS(0)_{iso} and NICS(1)_{iso} agree with an aromatic character.

As can be seen, this ionic compound does not result in a locally more aromatic compound as the X@C₂₈ compounds with group-4 atoms, for La@C₃₆ and the other compounds increase the aromaticity in some rings and decrease in others.

4 | CONCLUSIONS

Our results compare positively with experimental results. The binding energies is a good indicator of stability, their values can explain the lower abundance obtained for La@C₃₆ in comparison with Sc@C₃₆ and Y@C₃₆ although all of them are energetically favorable. Furthermore, Sc@C₃₆ and Y@C₃₆ were found in a high spin quartet state. In addition, their atom-cage bonds are different. For instance, La bonds ionically to the cage and is located at the fullerene's center, while Sc and Y bond covalently to a hexagonal ring; despite this, all metal atoms transferred charge to the cage. Their different behavior can be explained by the lower ionization energy of La in comparison with that of Sc and Y. Moreover, the small HOMO-LUMO gaps calculated for all M@C₃₆ show high reactivity. This results support the experimental observations and the proposed bottom-up growth mechanism. As well, the insertion of the endohedral atom chosen does not produce a more aromatic compound and thus aromaticity does not contribute to the stabilization. We expect that all other lanthanides will behave similar to La and will be located at the center of the cage.

ACKNOWLEDGMENTS

We thank the Computing and Information Technology Division of the National Autonomous University of Mexico (UNAM) for the computer resources (assignment SC16-1-IR-64), DGAPA for funding this research under project IN102616 and CONACYT for financial support (A. Miralrio scholarship).

REFERENCES

- [1] H. W. Kroto, J. R. Heath, S. C. O'Brien, R. F. Curl, R. E. Smalley, *Nature* **1985**, 318, 162.
- [2] J. Heath, S. O'Brien, Q. Zhang, Y. Liu, R. Curl, F. Tittel, R. Smalley, *J. Am. Chem. Soc.* **1985**, 107, 7779.
- [3] X. Lu, Z. Chen, *Chem. Rev.* **2005**, 105, 3643.
- [4] M. N. Chaur, F. Melin, A. L. Ortiz, L. Echegoyen, *Angew. Chem. Int. Ed.* **2009**, 48, 7514.
- [5] A. A. Popov, S. Yang, L. Dunsch, *Chem. Rev.* **2013**, 113, 5989.
- [6] P. Jin, C. Tang, Z. Chen, *Coord. Chem. Rev.* **2014**, 270–271, 89.
- [7] C. R. Wang, T. Kai, T. Tomiyama, T. Yoshida, Y. Kobayashi, E. Nishibori, M. Takata, M. Sakata, H. Shinohara, *Nature* **2000**, 408, 426.
- [8] H. W. Kroto, D. R. Walton, *Chem. Phys. Lett.* **1993**, 214, 353.
- [9] H. Prinzbach, A. Weiler, P. Landenberger, F. Wahl, J. Wörth, L. T. Scott, M. Gelmont, D. Olevano, B. V Issendorff, *Nature* **2000**, 407, 60.
- [10] D. M. Cox, D. J. Trevor, K. C. Reichmann, A. Kaldor, *J. Am. Chem. Soc.* **1986**, 108, 2457.
- [11] H. Kroto, *Science* **1988**, 242, 1139.
- [12] S. C. O'Brien, J. R. Heath, R. F. Curl, R. E. Smalley, *J. Chem. Phys.* **1988**, 88, 220.
- [13] H. Kroto, *Nature* **1987**, 329, 529.
- [14] T. Guo, M. Diener, Y. Chai, M. Alford, R. Haufler, S. McClure, T. Ohno, J. Weaver, G. Scuseria, R. Smalley, *Science* **1992**, 257, 1661.
- [15] H. Kietzmann, R. Rochow, G. Ganteför, W. Eberhardt, K. Vietze, G. Seifert, P. W. Fowler, *Phys. Rev. Lett.* **1998**, 81, 5378.
- [16] A. Koshio, M. Inakuma, Z. W. Wang, T. Sugai, H. Shinohara, *J. Phys. Chem. B* **2000**, 104, 7908.
- [17] Y. A. Yang, P. Xia, A. L. Junkin, L. A. Bloomfield, *Phys. Rev. Lett.* **1991**, 66, 1205.
- [18] P. W. Fowler, D. Manolopoulos, *An Atlas of Fullerenes*, Calderon: Oxford, **1995**.
- [19] Z. Chen, H. Jiao, A. Hirsch, W. Thiel, *Chem. Phys. Lett.* **2000**, 329, 47.
- [20] M. Côté, J. C. Grossman, M. L. Cohen, S. G. Louie, *Phys. Rev. Lett.* **1998**, 81, 697.
- [21] P. W. Fowler, T. Heine, K. M. Rogers, J. P. B. Sandall, G. Seifert, F. Zerbetto, *Chem. Phys. Lett.* **1999**, 300, 369.
- [22] J. C. Grossman, M. Côté, S. G. Louie, M. L. Cohen, *Chem. Phys. Lett.* **1998**, 284, 344.
- [23] E. Halac, E. Burgos, H. Bonadeo, *Chem. Phys. Lett.* **1999**, 299, 64.
- [24] A. Ito, T. Monobe, T. Yoshii, K. Tanaka, *Chem. Phys. Lett.* **2000**, 328, 32.
- [25] M. N. Jagadeesh, J. Chandrasekhar, *Chem. Phys. Lett.* **1999**, 305, 298.
- [26] D. S. Sabirov, R. G. Bulgakov, *JETP Lett.* **2010**, 92, 662.
- [27] L. F. Yuan, J. Yang, K. Deng, Q. S. Zhu, *J. Phys. Chem. A* **2000**, 104, 6666.
- [28] S. A. Varganov, P. V. Avramov, S. G. Ovchinnikov, M. S. Gordon, *Chem. Phys. Lett.* **2002**, 362, 380.
- [29] Y. Jin, C. Hao, *J. Phys. Chem. A* **2005**, 109, 2875.
- [30] C. Piskoti, J. Yarger, A. Zettl, *Nature* **1998**, 393, 771.
- [31] P. G. Collins, J. C. Grossman, M. Côté, M. Ishigami, C. Piskoti, S. G. Louie, M. L. Cohen, A. Zettl, *Phys. Rev. Lett.* **1999**, 82, 165.
- [32] H. S. Kang, *J. Phys. Chem. A* **2006**, 110, 4780.
- [33] Y. H. Cheng, C. Y. Zhang, J. Ren, K. Y. Tong, *Front. Phys.* **2016**, 11, 113101.

- [34] S. Du, Y. Huang, Y. Li, R. Liu, *J. Phys. Chem. B* **2002**, *106*, 4098.
- [35] M. Maruyama, N. T. Cuong, S. Okada, *J. Phys. Soc. Jpn.* **2015**, *84*, 84706.
- [36] Z. Chen, H. Jiao, A. Hirsch, W. Thiel, *Mol. Model. Annu.* **2001**, *7*, 161.
- [37] A. Kerim, *J. Mol. Model.* **2011**, *17*, 3257.
- [38] K. B. Shelimov, D. E. Clemmer, M. F. Jarrold, *J. Phys. Chem.* **1994**, *98*, 12819.
- [39] P. W. Dunk, M. Mulet-Gas, Y. Nakanishi, N. K. Kaiser, A. Rodríguez-Fortea, H. Shinohara, J. M. Poblet, A. G. Marshall, H. W. Kroto, *Nat. Commun.* **2014**, *5*, 5844.
- [40] T. Guo, R. E. Smalley, G. E. Scuseria, *J. Chem. Phys.* **1993**, *99*, 352.
- [41] A. Miralrio, L. E. Sansores, *Comput. Theor. Chem.* **2016**, *1083*, 53.
- [42] P. W. Dunk, N. K. Kaiser, M. Mulet-Gas, A. Rodríguez-Fortea, J. M. Poblet, H. Shinohara, C. L. Hendrickson, A. G. Marshall, H. W. Kroto, *J. Am. Chem. Soc.* **2012**, *134*, 9380.
- [43] K. B. Shelimov, M. F. Jarrold, *J. Am. Chem. Soc.* **1995**, *117*, 6404.
- [44] R. Klingeler, P. S. Bechthold, M. Neeb, W. Eberhardt, *J. Chem. Phys.* **2000**, *113*, 1420.
- [45] M. Mulet-Gas, L. Abella, P. W. Dunk, A. Rodríguez-Fortea, H. W. Kroto, J. M. Poblet, *Chem Sci.* **2015**, *6*, 675.
- [46] D. Manna, T. K. Ghanty, *J. Phys. Chem. C* **2013**, *117*, 17859.
- [47] H. Jia, L. Wang, P. Han, X. Liu, B. Xu, *Chem. J. Chin. Univ. Chin. Ed.* **2006**, *27*, 1958.
- [48] T. G. Lee, J. A. Ludlow, M. S. Pindzola, *J. Phys. B At. Mol. Opt. Phys.* **2012**, *45*, 135202.
- [49] I. Garg, H. Sharma, N. Kapila, K. Dharamvir, V. K. Jindal, *Nanoscale* **2011**, *3*, 217.
- [50] Y. H. Kim, Y. Zhao, A. Williamson, M. J. Heben, S. B. Zhang, *Phys. Rev. Lett.* **2006**, *96*, 016102.
- [51] R. Ahlrichs, M. Bär, M. Häser, H. Horn, C. Kölmel, *Chem. Phys. Lett.* **1989**, *162*, 165.
- [52] S. Grimme, S. Ehrlich, L. Goerigk, *J. Comput. Chem.* **2011**, *32*, 1456.
- [53] F. Weigend, R. Ahlrichs, *Phys. Chem. Chem. Phys.* **2005**, *7*, 3297.
- [54] **TURBOMOLE, V6.5: A Development of University of Karlsruhe and Forschungszentrum Karlsruhe GmbH, 1989–2007; TURBOMOLE GmbH: Karlsruhe, Germany, 2013.**
- [55] T. Lu, F. Chen, *J. Comput. Chem.* **2012**, *33*, 580.
- [56] M. J. Frisch, G. W. Trucks, H. B. Schlegel, G. E. Scuseria, M. A. Robb, J. R. Cheeseman, G. Scalmani, V. Barone, B. Mennucci, G. A. Petersson, H. Nakatsuji, M. Caricato, X. Li, H. P. Hratchian, A. F. Izmaylov, J. Bloino, G. Zheng, J. L. Sonnenberg, M. Hada, M. Ehara, K. Toyota, R. Fukuda, J. Hasegawa, M. Ishida, T. Nakajima, Y. Honda, O. Kitao, H. Nakai, T. Vreven, J. A. Montgomery, Jr., J. E. Peralta, F. Ogliaro, M. Bearpark, J. J. Heyd, E. Brothers, K. N. Kudin, V. N. Staroverov, R. Kobayashi, J. Normand, K. Raghavachari, A. Rendell, J. C. Burant, S. S. Iyengar, J. Tomasi, M. Cossi, N. Rega, J. M. Millam, M. Klene, J. E. Knox, J. B. Cross, V. Bakken, C. Adamo, J. Jaramillo, R. Gomperts, R. E. Stratmann, O. Yazyev, A. J. Austin, R. Cammi, C. Pomelli, J. W. Ochterski, R. L. Martin, K. Morokuma, V. G. Zakrzewski, G. A. Voth, P. Salvador, J. J. Dannenberg, S. Dapprich, A. D. Daniels, Ö. Farkas, J. B. Foresman, J. V. Ortiz, J. Cioslowski, D. J. Fox, *Gaussian 09, Revision D. 01*, Gaussian, Inc.: Wallingford CT, **2009**.
- [57] R. Dennington, T. Keith, J. Millam, *GaussView, Version 5*, Semichem Inc Shawnee Mission KS, **2009**.
- [58] F. Cimpoesu, S. Ito, H. Shimotani, H. Takagi, N. Drago, *Phys. Chem. Chem. Phys.* **2011**, *13*, 9609.
- [59] K. Hedberg, L. Hedberg, D. S. Bethune, C. Brown, H. Dorn, R. D. Johnson, M. De Vries, *Science* **1991**, *254*, 410.
- [60] D. Muigg, P. Scheier, K. Becker, T. Märk, *J. Phys. B At. Mol. Opt. Phys.* **1996**, *29*, 5193.
- [61] D. L. Huang, P. D. Dau, H. T. Liu, L. S. Wang, *J. Chem. Phys.* **2014**, *140*, 224315.
- [62] J. Aihara, *J. Phys. Chem. A* **1999**, *103*, 7487.
- [63] J. Aihara, *Phys. Chem. Chem. Phys.* **2000**, *2*, 3121.
- [64] J. C. Ma, D. A. Dougherty, *Chem. Rev.* **1997**, *97*, 1303.
- [65] Z. Chen, H. Jiao, M. Bühl, A. Hirsch, W. Thiel, *Theor. Chem. Acc.* **2001**, *106*, 352.
- [66] B. R. Sohnlein, S. Li, D. S. Yang, *J. Chem. Phys.* **2005**, *123*, 214306.
- [67] D. S. Yang, *J. Phys. Chem. Lett.* **2011**, *2*, 25.
- [68] Y. Liu, S. Kumari, M. Roudjane, S. Li, D. S. Yang, *J. Chem. Phys.* **2012**, *136*, 134310.
- [69] J. S. Lee, Y. Lei, S. Kumari, D. S. Yang, *J. Chem. Phys.* **2009**, *131*, 104304.
- [70] Y. Maeda, Y. Matsunaga, T. Wakahara, S. Takahashi, T. Tsuchiya, M. O. Ishitsuka, T. Hasegawa, T. Akasaka, M. T. H. Liu, K. Kokura, E. Horn, K. Yoza, T. Kato, S. Okubo, K. Kobayashi, S. Nagase, K. Yamamoto, *J. Am. Chem. Soc.* **2004**, *126*, 6858.
- [71] X. Lu, H. Nikawa, L. Feng, T. Tsuchiya, Y. Maeda, T. Akasaka, N. Mizorogi, Z. Slanina, S. Nagase, *J. Am. Chem. Soc.* **2009**, *131*, 12066.
- [72] M. Hachiya, H. Nikawa, N. Mizorogi, T. Tsuchiya, X. Lu, T. Akasaka, *J. Am. Chem. Soc.* **2012**, *134*, 15550.
- [73] M. Weller, T. Overton, J. Rourke, F. Armstrong, *Inorganic Chemistry*, OUP Oxford **2014**.
- [74] E. Nishibori, M. Takata, M. Sakata, M. Inakuma, H. Shinohara, *Chem. Phys. Lett.* **1998**, *298*, 79.
- [75] M. Takata, B. Umeda, E. Nishibori, M. Sakata, Y. Saitot, M. Ohno, H. Shinohara, *Nature* **1995**, *377*, 46.
- [76] E. Nishibori, M. Takata, M. Sakata, H. Tanaka, M. Hasegawa, H. Shinohara, *Chem. Phys. Lett.* **2000**, *330*, 497.
- [77] K. Kobayashi, S. Nagase, *Chem. Phys. Lett.* **1998**, *282*, 325.
- [78] T. Jayasekharan, T. K. Ghanty, *J. Phys. Chem. C* **2010**, *114*, 8787.
- [79] D. Manna, T. Jayasekharan, T. K. Ghanty, *J. Phys. Chem. C* **2013**, *117*, 18777.

SUPPORTING INFORMATION

Additional Supporting Information may be found online in the supporting information tab for this article.

How to cite this article: A. Miralrio, L. E. Sansores. Structures, stabilities, and electronic properties of fullerene C₃₆ with endohedral atomic Sc, Y, and La: A dispersion-corrected DFT study. *Int. J. Quantum Chem.* **2017**;117:e25335. <https://doi.org/10.1002/qua.25335>